Available online at www.sciencedirect.com
ScienceDirect
Journal of Organometallic Chemistry 692 (2007) 2582–2592
Journal of Organometallic Chemistry
www.elsevier.com/locate/jorganchem

Synthesis under self-controlled reaction conditions: Reaction of tetraamminezinc(II) chloride with 3,5-dimethyl-1-thiocarboxamide pyrazole ☆

Attila Kovács [a,*], Katalin Mészáros Szécsényi [b], Vukadin M. Leovac [b], Zoran D. Tomić [c], György Pokol [d]

[a] Research Group for Materials Structure and Modeling of the Hungarian Academy of Sciences, Budapest University of Technology and Economics, H-1111 Budapest, Szt. Gellért tér 4, Hungary
[b] Faculty of Sciences, University of Novi Sad, Department of Chemistry, Trg Dositeja Obrdovića 3, 21000 Novi Sad, Serbia and Montenegro
[c] Institute of Nuclear Sciences "Vinča", P.O. Box 522, 11001 Belgrade, Serbia and Montenegro
[d] Institute of Inorganic and Analytical Chemistry, Budapest University of Technology and Economics, H-1521 Budapest, Szt. Gellért tér 4, Hungary

Received 6 November 2006; received in revised form 23 February 2007; accepted 2 March 2007
Available online 12 March 2007

Abstract

The trinuclear $[Zn_3(Hdmpz)_2(dmpz)_4(NCS)_2]$ complex (*Hdmpz*: 3,5-dimethylpyrazole) has been synthesized by the reaction of tetraamminezinc(II) chloride with 3,5-dimethyl-1-thiocarboxamidepyrazole. The ammonia evolving gradually from $[Zn(NH_3)_4]Cl_2$ ensured a mild gradually increasing basic pH during the synthesis which caused a cleavage of the 1-*N*-substituent. Moreover, the changing pH controlled the pyrazolate anion–neutral ligand equilibrium, and in this way the formation of the precipitate complex. The structure of the complex was investigated by X-ray diffraction and quantum chemical computations. The complex was characterized in detail by FT-IR-spectroscopy and thermal analysis. The bonding interactions between Zn^{2+} and the ligands were analysed on the basis of the computed data.

Keywords: Crystal growth; XRD; FT-IR; Thermal analysis; DFT computations

1. Introduction

Single crystals are demanded in various fields of chemical research and industry. In spite of the available routine techniques [1,2], however, single crystals of transition metal complexes are often difficult to prepare. In the presented work we used a method convenient for the synthesis of transition metal complexes with anionic ligands. The main point of the method is that the metal ion is initially in the form of an ammonia complex, $[M(NH_3)_x]^{n+}$. The evaluation of NH_3 during the ligand exchange (Eq. (1)) leads to a gradual variation of pH, which controls the anion–neutral ligand equilibrium and through it the rate of complex formation.

$$[M(NH_3)_x]^{n+} + nHL \leftrightarrow [ML_n] + n NH_4^+ + (x-n)NH_3 \quad \text{or} \quad (1a)$$

$$[M(NH_3)_x]^{n+} + mHL + (n-m)A^- \leftrightarrow ML_mA_{(n-m)} + mNH_4^+ + (x-m)NH_3 \quad (1b)$$

The method is known in analytical chemistry as precipitation from homogeneous solution [3] and is used to obtain complexes in crystalline form for gravimetric analy-

☆ This paper is Part 24 in the series of our studies on Transition Metal Complexes with Pyrazole Based Ligands. Part 23 V.M. Leovac, R. Petković, A. Kovács, G. Pokol, K. Mészáros Szécsényi, J. Therm. Anal. Calorim. (2007) in press.

* Corresponding author. Present address: Institute of Inorganic and Analytical Chemistry, Budapest University of Technology and Economics, H-1111 Budapest, Szt. Gellért tér 4, Hungary. Tel.: +36 1 463 2278; fax: +36 1 463 3408.
E-mail addresses: akovacs@mail.bme.hu (A. Kovács), mszk@uns.ns.ac.yu (K.M. Szécsényi).

0022-328X/$ - see front matter © 2007 Elsevier B.V. All rights reserved.
doi:10.1016/j.jorganchem.2007.03.003

sis. Advantage of the method is that the crystal formation is determined by self-controlling the rate of the chemical reaction, as the rate increases rapidly when the evolved NH_3 makes the solution more basic. The small number of the initial crystal nuclei favours the formation of a few well-defined single crystals.

We applied the above procedure to the reaction of $ZnCl_2$ with 3,5-dimethyl-1-thiocarboxamidepyrazole. Pyrazole derivatives can easily form anions by elimination of the pyrrole NH or any acidic hydrogen of substituents (if present). Moreover, 1-*N* substituents tend also to split off under basic conditions [4–6]. Pyrazoles establish usually strong monodentate or chelate complexes with transition metals, which complexes have numerous practical and theoretical applications [4,5,7].

In the title reaction we obtained single crystals of the trinuclear $[Zn_3(Hdmpz)_2(dmpz)_4(NCS)_2]$ complex (*Hdmpz* = 3,5-dimethylpyrazole). The complex is characterized by X-ray diffraction, FT-IR spectroscopy and thermal analysis. We report furthermore an analysis of the metal–ligand interactions by quantum chemical computations.

2. Experimental and computational details

2.1. Synthesis of the complex

The synthesis was performed using a metal-to-ligand molar ratio of 1:2. The solutions were prepared by dissolving 0.07 g (0.5 mmol) of zinc(II) chloride in 2 cm^3 cc. NH_3 (resulting in the formation of $[Zn(NH_3)_4]^{2+}$) with addition of 5 cm^3 EtOH and dissolving 0.15 g (1 mmol) of 3,5-dimethyl-1-thiocarboxamidepyrazole (3,5-dimethyl-1H-pyrazole-1-carbothioamide, *dmpzCSNH*$_2$) in 5 cm^3 EtOH. The two solutions were mixed at room temperature. The complex formation started almost immediately after the mixing and the precipitate consisted mainly of single crystals. After 3 h the white precipitate was vacuum filtered, washed with cold EtOH and air dried. When the crystals were left to stand for more than 3 h in the solution, we observed their dissolution due probably to the change of pH (evaporation of NH_3 from the solution). Additional experiments in various solvents (EtOH, MeOH, Me_2CO) but without ammonia failed to give any precipitate.

Yield: 0.05 g (~40%). Elemental analysis data, Calc.: C, 43.42; H, 5.01; N, 22.16. Found: C, 43.5; H, 4.8; N, 22.1%. Molar conductivity in DMF, $\lambda_M = 44.0$ S cm^2 mol^{-1}.

2.2. Elemental analysis

(C, H, N) was performed by standard methods.

2.3. X-ray structure determination

A single crystal of the complex with approximate dimensions of $0.10 \times 0.10 \times 0.12$ mm^3 was selected for data collection. The data were collected on a Bruker AXS SMART diffractometer with an APEX CCD detector, equipped with a Bede Microsource® X-ray generator, using Mo Kα radiation. A full sphere of data was collected with a frame width of 0.3° and a counting time of 40 s per frame. A multiscan absorption correction [8] was applied to the raw data and the resulting R_{int} was 7.1%. Frames were integrated using the program SAINT [9] The crystal structure was solved by direct methods using the SIR92 software [10] and refined using the Oxford Crystals suite [11]. The positions and anisotropic atomic displacement parameters of all non-hydrogen atoms were refined; hydrogen atoms were located from difference Fourier maps and refined isotropically using restraints. Molecular graphics were created using the program ORTEP [12].

2.4. FT-IR spectroscopy

The FT-IR spectra were recorded at room temperature using KBr pellets in the range of 4000–450 cm^{-1} on a Perkin–Elmer System 2000 FT-IR spectrometer equipped with an MCT detector using a co-addition of 16 scans. The far-IR (650–50 cm^{-1}) measurements were carried out with polyethylene pellets and DTGS detector using 128 scans. The spectra were recorded with a resolution of 4 cm^{-1}.

2.5. Conductivity measurements

Molar conductivity of freshly prepared 10^{-3} mol/dm^3 solutions in DMF was measured at room temperature using a digital conductivity meter Jenway 4010.

2.6. Thermal analysis

Thermal analysis was performed using a DuPont 1090 TA system with sample masses of about 5 mg and were performed in both argon and air atmospheres at a heating rate of 10 K/min. In the thermogravimetric measurements platinum crucible was employed, while the DSC curves were recorded up to 600 K using an open aluminium pan sample holder with an empty aluminium pan as reference. The EGD measurement was accomplished on a DuPont 916 TEA (Thermal Evolution Analyser) instrument in a flowing nitrogen atmosphere and a heating rate of 8 K min^{-1} to 600 K.

2.7. DFT computations

The quantum chemical computations were carried out with the GAUSSIAN 03 program package [13] using the Becke3–Lee–Yang–Parr (B3-LYP) [14,15] exchange-correlation functional. The relativistic effective core potential and its [21/11/41] valence basis set of Hay and Wadt [16] was used for Zn, extended with a single set of *f* type polarisation functions ($\alpha = 3.031$) [17]. The 6-31G** basis set was applied for H, C, N and S. The minimum character of the optimised structures was verified by frequency calculations. The dissociation energies were evaluated from the

computed absolute energies after corrections for zero-point vibrational energy (ZPE) and basis set superposition error (BSSE), the latter estimated by the counterpoise method [18].

3. Results and discussion

3.1. Formation and general properties of $[Zn_3(Hdmpz)_2(dmpz)_4(NCS)_2]$

In our previous studies of transition metal complexes with pyrazole-based ligands we observed often the elimination of the 1-*N*-substituent resulting in the formation of 1-*H*-pyrazoles [4–6]. Sometimes the elimination took place only in a portion of the ligand molecules and in the reaction mixed complexes with both 1-*H*-pyrazole and 1-*N*-substituted pyrazole ligands in the complex were obtained [5,19–21].

The 1-*N* thiocarboxamide substituent in 3,5-dimethyl-1-thiocarboxamidepyrazole (*dmpz*$CSNH_2$), the thiocarboxamide group, is particularly labile. Though *dmpz*$CSNH_2$ is stable at room temperature for months, it decomposes at somewhat higher temperatures to 3,5-dimethylpyrazole (*Hdmpz*) and HNCS. A similar decomposition can occur in basic (e.g. NH_3) solution as presented in Scheme 1. The formed 3,5-dimethylpyrazolate anion (*dmpz*) is a bidentate ligand with the two nitrogens as possible donors.

$$3[Zn(NH_3)_4]^{2+} + 6dmpzCSNH_2 = [Zn_3(Hdmpz)_2(dmpz)_4(NCS)_2] + 10NH_4^+ + 4NCS^- + 2NH_3 \quad (2)$$

The title reaction resulted in the trinuclear $[Zn_3(Hdmpz)_2(dmpz)_4(NCS)_2]$ complex according to Eq. (2). Its molecular structure determined by X-ray diffraction is shown in Fig. 1. The complex has a compact $[Zn_3(dmpz)_4]^{2+}$ core stabilized by strong ionic and donor–acceptor Zn–N interactions. The core includes four deprotonated bidentately coordinated *dmpz* ligands arranged in a tetrahedral coordination around the middle Zn^{2+}. The tetrahedral coordination of each terminal Zn^{2+} ion is established by an ionic bond with an NCS^- (fulfilling the neutrality requirement) and a donor–acceptor bond with the pyridine nitrogen of a *Hdmpz* ligand. The presence of *Hdmpz* is the consequence of the mild basic pH of the NH_3 solution. Identified by its smell, part of the evolved NH_3 evaporated from the solution.

The formation of the $[Zn_3(Hdmpz)_2(dmpz)_4(NCS)_2]$ complex can partly be interpreted upon the HSAB principle [22–24] in accordance with our earlier experience with similar systems [4,7,21]. It explains, why the chloride ions (hard bases) of $ZnCl_2$ are replaced by the isothiocyanate ions (medium hard at the N side) on the medium hard acid Zn^{2+}. A coordination of NCS^- through the sulphur atom is less favoured because of its soft base character. Steric effects, which could lead to deviations from the HSAB principle, seem to be less important in the title complex.

There are several examples how changes in the pH and counter-ions of Zn^{2+} can influence the product of complex formation with pyrazole-type ligands. Masciocchi et al. obtained a polymeric $[Zn(pz)_2]_x$ complex from $ZnCl_2$ and pyrazole (*Hpz*) in aqueous NH_3 solution [25]. Because of the excess NH_3 the precipitate complex was obtained in

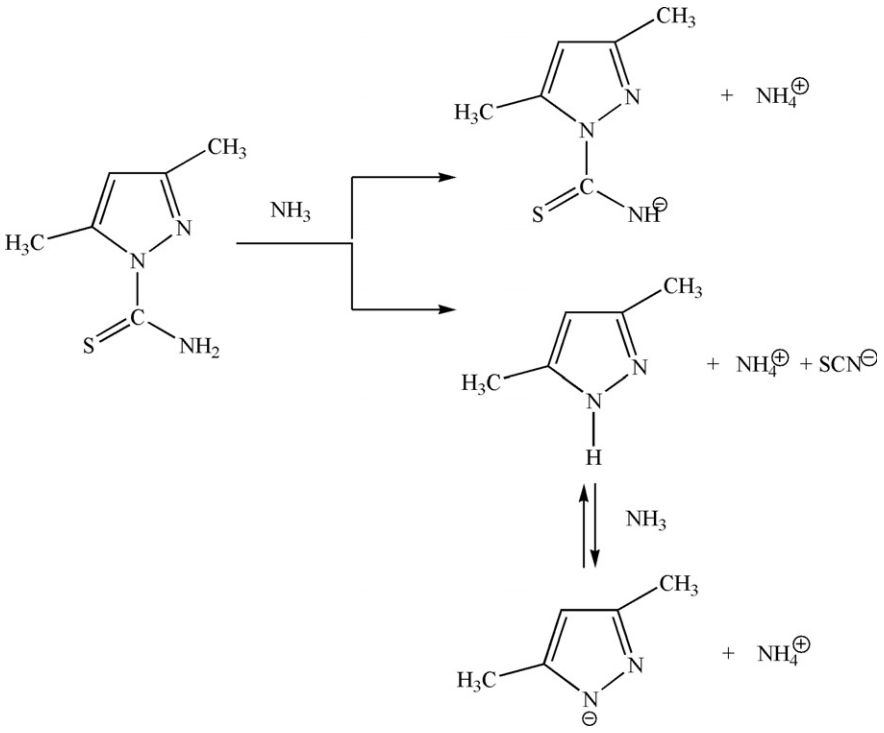

Scheme 1.

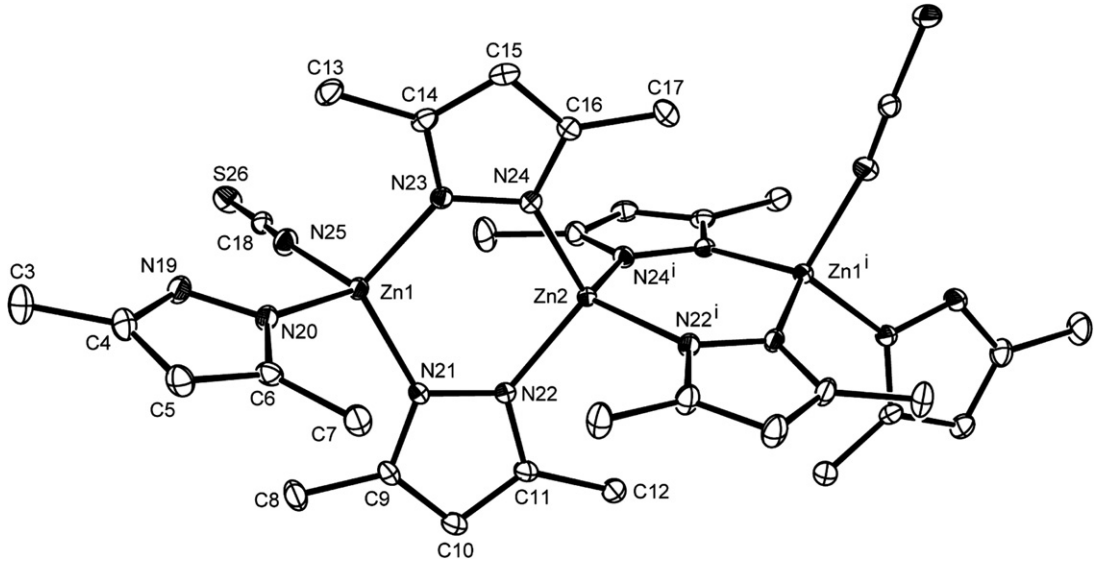

Fig. 1. Structure and atom numbering of the $[Zn_3(Hdmpz)_2(dmpz)_4(NCS)_2]$ unit from the X-ray diffraction analysis ($i = -x + 1/2, -y + 1/2, z$).

microcrystalline form. The binuclear $[Zn_2(Hdmpz)_2(dmpz)_2]$ complex has been synthesized by Ehlert et al. heating zinc metal with excess of *Hdmpz* in concentrated acetonic solution under O_2 [26]. While no basis was introduced into the reaction mixture, the red-ox processes could generate mild basic conditions for a partial deprotonation of *Hdmpz*. In our recent study the reaction of $Zn(OAc)_2$ (OAc = acetate) with 4-acetyl-3-amino-5-methylpyrazole (HL^1) in a neutral MeOH–DMF solution gave single crystals of the binuclear complex $[Zn_2(HL^1)_2(L^1)_2(OAc)_2]$ [27]. In the latter case, the acetate ion is a Brønsted base and in this way it is able to deprotonate the ligand. Note that neither of the above mentioned reactions was carried out in a self-controlled manner.

Among the general properties of the $[Zn_3(Hdmpz)_2(dmpz)_4(NCS)_2]$ complex we should mention its rather low solubility in water and alcohols, referring also to its polynuclear structure. The molar conductivity in DMF (44.0 S cm^2 mol^{-1}) may suggest a partial exchange of an NCS^- ion with a solvent molecule [28].

Table 1
Crystallographic details for the $[Zn_3(Hdmpz)_2(dmpz)_4(NCS)_2]$ complex

Chemical formula	$C_{32}H_{44}N_{14}S_2Zn_3$
Molecular weight (amu)	885.09
Crystal system	orthorombic
Space group	*Pccn*
a (Å)	18.064(2)
b (Å)	12.9962(15)
c (Å)	17.140(2)
α (°)	90
β (°)	90
γ (°)	90
V (Å^3)	4023.9(8)
Z	4
T (K)	120
d_{calc} (g/cm^{-3})	1.461
μ (mm^{-1})	1.920
Total number of reflections	51343
Number of unique reflections	5870
Number of observed reflections ($I > 2\sigma$)	3470
Number of parameters refined	319
R_{int} (%)	7.1
R (%) for $I > 2\ \sigma$	4.37
wR (%)	10.85

3.2. Crystal and molecular structure

The crystallographic details are given in Table 1, while selected bond lengths and angles are listed in Table 2.

The crystal structure of $[Zn_3(Hdmpz)_2(dmpz)_4(NCS)_2]$ is built up of discrete trinuclear units (cf. Fig. 1). The central zinc atom, Zn2, which is located on a twofold axis, is bridged to the symmetry-related Zn1 atoms by *dmpz* molecules in exo-bidentate mode. The coordination sphere of the terminal Zn1 atoms is completed by a monodentately coordinated *Hdmpz* ligand and an isothiocyanate anion. Both symmetrically unique Zn atoms are coordinated in a distorted tetrahedral fashion with angles ranging from 102.3(1)° to 111.9(1)°. The ligand-bridged Zn···Zn nonbonding distance is 3.602(6) Å. The different coordination modes of the ligands are reflected in their geometrical parameters. The largest difference is observed in the N–N distances, which are longer in the bridging *dmpz* (1.383(4) and 1.386(4) Å) compared to that of the terminal *Hdmpz* ligands (1.361(4) Å). The same pattern of difference was previously observed in the crystal structure of $[Zn_2(HL^1)_2(L^1)_2(OAc)_2]$ [27].

Since the rings of the pyrazolyl ligands are aromatic, it would be interesting to see how the different modes of coordination influence the overall aromatic character of the pyrazole ring. We evaluated the aromaticity index based on the Harmonic Oscillator Model of Aromaticity (HOMA) [29] and found that the terminal *Hdmpz* ligands express slightly larger aromatic character (0.924) as compared to the bridging *dmpz* ones (0.845).

Table 2
Selected bond lengths (Å) and angles (°) in $[Zn_3(Hdmpz)_2(dmpz)_4(NCS)_2]$[a]

	Bond lengths			Bond angles	
	X-ray	Computed[b]		X-ray	Computed[b]
Zn2–N24	1.992(3)	2.078	N24–Zn2–N22	109.5(1)	108.6
Zn2–N22	1.989(3)	2.088	N24–Zn2–N24^i	111.9(2)	109.1
Zn1–N23	1.972(3)	2.043	N24–Zn2–N22^i	109.8(1)	110.9
Zn1–N25	1.974(3)	2.035	N22–Zn2–N22^i	106.1(2)	108.8
Zn1–N21	1.975(3)	2.050	N23–Zn1–N25	110.2(1)	116.1
Zn1–N20	2.034(3)	2.161	N23–Zn1–N21	111.9(1)	111.6
S26–C18	1.627(4)	1.613	N25–Zn1–N21	111.4(1)	115.3
N23–N24	1.383(4)	1.375	N23–Zn1–N20	110.1(1)	110.0
N23–C14	1.353(4)	1.352	N25–Zn1–N20	102.3(1)	91.4
N24–C16	1.343(4)	1.351	N21–Zn1–N20	110.6(1)	110.7
N25–C18	1.152(5)	1.195	Zn1–N23–N24	123.7(2)	124.0
N21–N22	1.386(4)	1.375	Zn1–N23–C14	128.6(2)	127.6
N21–C9	1.343(4)	1.351	N24–N23–C14	107.7(3)	108.4
N19–N20	1.361(4)	1.356	N23–N24–Zn2	124.4(2)	124.8
N20–C6	1.335(4)	1.341	N23–N24–C16	108.0(3)	108.1
N19–C4	1.341(5)	1.351	Zn2–N24–C16	127.6(2)	126.2
N22–C11	1.338(4)	1.350	Zn1–N25–C18	163.0(3)	157.6
C15–C16	1.394(5)	1.398	Zn1–N21–N22	121.8(2)	124.0
C14–C15	1.383(5)	1.395	Zn1–N21–C9	130.0(2)	127.4
C16–C17	1.502(6)	1.500	N22–N21–C9	108.1(3)	108.5
C11–C12	1.502(5)	1.500	Zn1–N20–C6	131.6(2)	140.2
C10–C11	1.397(5)	1.397	N19–N20–C6	105.8(3)	106.1
C8–C9	1.495(5)	1.500	N20–N19–C4	111.7(3)	112.3
C9–C10	1.377(6)	1.396	N21–N22–Zn2	126.0(2)	125.0
C13–C14	1.500(5)	1.500	N21–N22–C11	107.7(3)	108.0

[a] For the numbering of atoms see Fig. 1. Symmetry code: $i = -x + 1/2, -y + 1/2, z$.
[b] Computed at the B3LYP/6-31G** level using a relativistic effective core potential for Zn.

Distances of the central Zn2 atom from the bridging *dmpz* nitrogens (1.989(3)/1.992(3) Å) are somewhat longer than the related distances of the terminal Zn1 atoms (1.975(3)/1.972(3) Å). The terminal *Hdmpz* molecules coordinate through the pyridine nitrogen atom to Zn1 at a distance of 2.034(3) Å. The dihedral angle between the mean planes of two symmetrically unique bridging *dmpz* ligands is 18.1°. The Zn1–N21–N22–Zn2–N24–N23 six-membered metallocycle possesses a boat conformation with Zn1 and Zn2 out of the N21–N22–N23–N24 mean plane (maximum deviation of the nitrogens from the reference plane is 0.02 Å) by 0.24 and 0.16 Å, respectively. The Zn–N(NCS) bond length (1.974(3) Å) is similar to that observed in the crystal structure of bis(*Hdmpz*)-bis(isothiocyanato)-zinc(II) (1.934(3) Å) [30], but longer than the Zn–N(NCS) distance found in (tris-(3-*t*-butylpyrazolyl)hydroborato)-isothiocyanato–zinc(II) (1.893(4) Å) [31]. The difference may partly be ascribed to N–H···S intermolecular hydrogen bonding interactions missing from the latter complex. Such intermolecular hydrogen bonds are responsible for the self-assembly of the trinuclear $[Zn_3(Hdmpz)_2(dmpz)_4(NCS)_2]$ units in the crystal, running in chain along the *b*-axis of the unit cell (cf. Fig. 2. N19–H34···S26^i: H···S = 2.6, N–H···S = 155; $i = 0.5 - x, 0.5 - y, z$). Note that the intramolecular N–H···N distance of 2.8 Å indicates a very weak interaction between the *Hdmpz* and NSC^- ligands in the complex.

The computations reproduced the trinuclear molecular structure of the $[Zn_3(Hdmpz)_2(dmpz)_4(NCS)_2]$ complex, supporting that it is not merely the result of solid-phase effects. The stability of this structure is further supported by the large computed dissociation energies (vide infra). There are, however, some significant differences between the geometrical parameters of the crystal and computed structure, which can be attributed partly to the single-molecule model of the computations in contrast to the found four-molecule unit cells in the crystal, to the neglect of other intermolecular interactions by the computations and to the approximations involved in the used theoretical level.

Thus, the computations underestimated the Zn–N interactions resulting in characteristically longer Zn–N_{Py} distances (2.05–2.09 Å vs. 1.97–1.99 Å in the crystal for the inner *dmpz*, while 2.16 Å vs. 2.03 Å for the terminal *Hdmpz* units). The intramolecular N–H···N(NCS) hydrogen bonding interaction is considerably overestimated by the computations predicting a H···N distance of 2.1 Å in contrast to the 2.8 Å in the crystal. Regarding the NCS^- ligand, its Zn–N distance is overestimated by 0.06 Å, the N=C bond by 0.04 Å. On the other hand, the C=S distance differs only by 0.015 Å (underestimated by the computations). A better agreement has been achieved for the bond distances in the *dmpz* and *Hdmpz* ligands: most of them agree within 0.01 Å. Similarly, the X-ray and computed bond angles agree generally within 1° for the *dmpz*

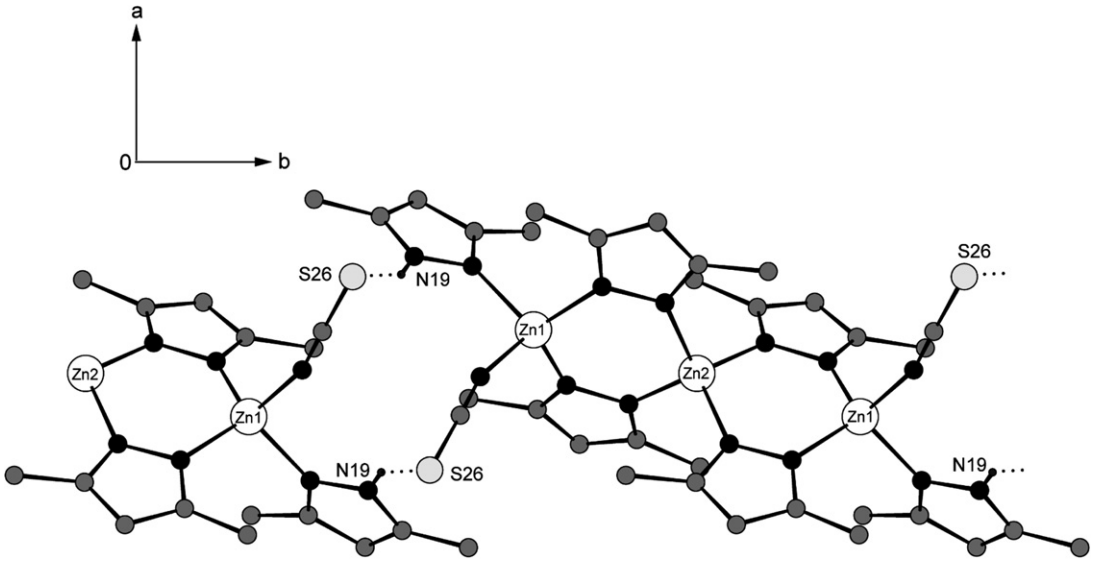

Fig. 2. A part of the crystal structure of $[Zn_3(Hdmpz)_2(dmpz)_4(NCS)_2]$ showing the association of molecules into a chain running along the *b*-axis. H atoms not involved in hydrogen bonds have been omitted for clarity.

and *Hdmpz* ligands, whereas can deviate up to 11° for the bond angles including the Zn^{2+} ions. The largest deviations are observed in the case of the terminal *Hdmpz* and NCS^- ligands being the most flexible parts of the complex, hence more sensitive on the crystal packing effects.

3.3. FT-IR spectra

The assignment of the IR spectra (Fig. 3, Table 3) was based on the computed wavenumbers and IR intensities at the B3LYP/6-31G** level, visualizing the normal modes by the Molden3.8 program [32]. From the expected 279 fundamentals of the complex 52 bands could be distinguished in our spectra as a result of extensive overlap between close-lying fundamentals, where the numerous weak bands are hidden by neighbouring stronger ones.

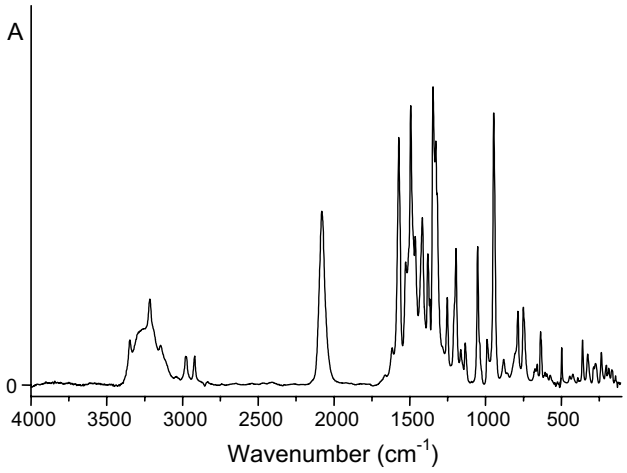

Fig. 3. FT-IR spectrum of solid $[Zn_3(Hdmpz)_2(dmpz)_4(NCS)_2]$.

The computations and comparison with the literature IR data of transition metal complexes with pyrazole derivatives [7,33,34] facilitated a reliable assignment of the present IR spectra given in Table 3. We found an unexpectedly good agreement between the computed and experimental frequencies for several bands in the 1616–1200 cm^{-1} range as a probable result of fortunate cancellation of errors of our computational model (harmonic approximation, single-molecule model, approximations of the theoretical level). The only noteworthy contradiction between the measurements and computation is the strong band at 945 cm^{-1}, which has no analogue in this region of the computed spectrum. The possibility of an impurity in such a large amount could be excluded by elemental analysis and by the (reproduced) IR spectrum of samples from repeated syntheses. Literature spectra of 3,5-dimethylpyrazole [34] and complexes with related pyrazole derivatives [7,33] did not show a strong band in this region implying that it may belong to the NCS^- ligand. However, the C═S stretching mode of NCS^- coordinated to a transition metal by N appears between 690 and 840 cm^{-1} [35–37], in good agreement with our computed value of 877 cm^{-1} for the title complex. The 945 cm^{-1}-band may be assigned to a methyl rocking mode red-shifted and gained considerable intensity in the four-molecule unit cell with respect to the normal mode of the single molecule modelled by our computations. A Fermi resonance effect may also contribute to the differences between the observed band and the computed data, but the other band of the Fermi pair cannot unambiguously be identified in this crowded region of the spectrum.

The vibrations of the pyrazole ring and the methyl substituents correlate well with literature data [33,38]. The measured frequency of the pyrazole CH stretching (3144 cm^{-1}) supports clearly the aromaticity of the *dmpz*

Table 3
Characteristic bands[a] in the FT-IR spectra of $[Zn_3(Hdmpz)_2(dmpz)_4(NCS)_2]$

Experimental	Calculated[b]		
	Frequency	IR intensity	Assignment[c]
3347 s	3500	578	νN–H
3215 s	3500	407	νN–H
3144 w	3265	13	νC_{Py}–H
2979 m	3111	31	$\nu_{as}CH_3$
2973 sh	3105	53	$\nu_{as}CH_3$
2919 m	3045	274	$\nu_s CH_3$
2080 vs	2110	2863	νNCS(N ≡ C)
1616 m	1619	84	νPy, δC_{Py}–H, βN–H,
1572 vs	1575	249	νPy, δC_{Py}–H
1526 m	1546	50	νPy, $\delta_{as}CH_3$
1493 vs	1517	102	νPy, $\delta_{as}CH_3$, βN–H
1475 sh	1508	12	$\delta_{as}CH_3$
1463 m	1496	68	$\delta_{as}CH_3$
1416 s, br	1468	350	νPy, $\delta_{as}CH_3$
1380 m	1449	50	νPy, $\delta_s CH_3$, βN–H
1367 sh	1424	21	$\delta_s CH_3$
1346 vs	1374	293	νPy
1328 s	1316	119	νPy, βN–H
1252 m	1220	163	νPy(N–N)
1194 s	1184	128	νPy(N–N)
1133 m	1105	16	βPy, $\delta_{as}CH_3$
1051 s	1053	265	νPy, βPy
1038 sh	1046	44	νPy, βPy
989 m	1003	35	$\delta_{as}CH_3$(rock)
945 s	1001	12	$\delta_{as}CH_3$(rock)
879 w	877	12	νNCS(C═S)
805 sh	820	76	γC–H_{Py}
785 s	799	68	γC–H_{Py}
750 s	764	44	νC–CH_3, βPy
743 sh	754	11	νC–CH_3, βPy
671 w	673	1	τPy
636 m	619	11	τPy, γN–H
595 w	596	5	βPy
481 m	509	26	δNCS
422 w	447	15	βC–CH_3
400 m	427	35	βC–CH_3
363 w	348	75	γC–CH_3, τPy
329 s	332	101	βC–CH_3, γC–CH_3
291 s	286	49	βC–CH_3, νZn–N_{NCS}
283 sh	270	101	νZn–N_{NCS}, βC–CH_3
251 sh	237	43	βC–CH_3, νZn_1–N_{Py}, νZn_2–N_{Py}
248 m	231	85	νZn_2–N_{Py}, βC–CH_3, νZn_1–N_{Py}
234 m	215	34	νZn_2–N_{Py}, νZn_1–N_{Py}
224 sh	205	46	νZn_1–N_{Py}, βC–CH_3
198 sh	196	15	γZn–Py (butterfly)
191 m	188	66	γC–CH_3
154 m	154	14	βZn–N_{NCS}, βZn–N_{Py}
137 w	148	14	βZn–N_{Py}
114 w	118	10	τCH_3
89 w	99	0.3	τCH_3 or lattice
70 w	63	0.4	γN_{Py}–Zn or lattice
57 w	58	0.5	γN_{Py}–Zn or lattice

[a] In cm^{-1}. The abbreviations for the band intensities vs, s, m, w, sh mean very strong, strong, medium, week and shoulder, respectively.

[b] Computed at the B3LYP/-31G** level using a relativistic effective core potential for Zn. The computed IR intensities of the close lying fundamentals representing identical vibrations were added together.

[c] The abbreviations ν, β, δ, γ, τ, s, as, Py mean stretch, in-plane bend, deformation, out-of-plane bend, torsion, symmetric, asymmetric, pyrazole ring vibrations, respectively.

rings. The Zn–N_{Py} stretching modes appear between 220 and 250 cm^{-1}, somewhat lower than the respective modes of pyridine complexes (280–300 cm^{-1}) [39]. Most Zn–N stretching vibrations are mixed with the C–CH_3 in-plane bending of the methyl groups. The in-plane Zn–N bending modes of the complex appear around 150 cm^{-1}, while the out-of-plane Zn–N bendings below 100 cm^{-1} (cf. Table 3). We could identify the metal–ligand Zn–N_{NCS} stretching vibrations around 290 cm^{-1}. Note that although we could reasonably correlate three bands below 100 cm^{-1} with computed fundamentals, these bands could also alternatively be assigned to lattice vibrations.

3.4. Bonding properties

The title complex shows very interesting bonding properties. The general chemical intuition would suggest four single (ionic) bonds with the deprotonated nitrogens of the four *dmpz* ligands, four weaker donor–acceptor interactions with the other (pyridine-type) nitrogens of these *dmpz* ligands and two donor–acceptor interactions with the pyridine-type nitrogens of the terminal *Hdmpz* ligands. Analysis of the Zn–N distances, atomic charges and hyperconjugation effects shows, however, that the bonding situation is more complex. First of all, the Zn–N_{Py} distances are not so much different: they vary within 0.04 Å in the computed while within 0.02 Å in the solid-phase structure for the inner $[Zn_3dmpz_4]^{2+}$ moiety. This indicates that instead of the supposed strong ionic and weaker donor–acceptor Zn–N interactions, all the Zn–N bonds in the inner moiety are of similar strength. On the other hand, the Zn–N interactions with the terminal *Hdmpz* ligands are, as expected, much weaker (cf. these longer Zn–N distances in Table 2).

We computed the energies of various dissociation reactions of the complex into smaller fragments as given in Table 4. They justify the strong ionic bond between Zn^{2+} and the NCS^- ions (547.8 kJ/mol) [40] as well as the expected weak donor–acceptor interaction between Zn^{2+} and the terminal *Hdmpz* ligands (104.2 kJ/mol). From the data of Table 4 the average bonding energy for a Zn–N bond within the $[Zn_3dmpz_4]^{2+}$ moiety can be evaluated as 430.6 kJ/mol.

The most important characteristics of the natural atomic charges (Table 5) are the values of the zinc ions close to +2

Table 4
Computed dissociation energies[a] of $[Zn_3(Hdmpz)_2(dmpz)_4(NCS)_2]$

Dissociation products	ΔE
$[Zn_3(Hdmpz)_2(dmpz)_4]^{2+} + 2NCS^-$	1095.7
$[Zn_3(dmpz)_4(NCS)_2] + 2Hdmpz$	208.5
$3Zn^{2+} + 2NCS^- + 2Hdmpz + 4dmpz^-$	4749.0

[a] Computed at the B3LYP/-31G** level using a relativistic effective core potential for Zn. The data (kJ/mol) refer to 0 K and are corrected for zero-point vibrational energy and basis set superposition error.

Table 5
Selected results[a] of the natural bond orbital analysis of $[Zn_3(Hdmpz)_2(dmpz)_4(NCS)_2]$

Property	
qZn2	+1.61
qZn1	+1.60
qN20	−0.50
qN19	−0.34
qN23	−0.59
qN24	−0.55
qN21	−0.58
qN22	−0.56
qN25	−0.99
qC18	+0.22
qS26	−0.11
$E^{(2)}$ LP(N24) → s(Zn2)	193.4
$E^{(2)}$ LP(N23) → s(Zn1)	250.9
$E^{(2)}$ LP(N25) → s(Zn1)	216.0
$E^{(2)}$ LP(N20) → s(Zn1)	159.3
$E^{(2)}d$(Zn2) → π*(N24–C16)	6.2
$E^{(2)}d$(Zn2) → π*(N24–N23)	4.6
$E^{(2)}d$(Zn1) → π*(N24–N23)	5.3
$E^{(2)}d$(Zn1) → π*(N23–C14)	7.9
$E^{(2)}d$(Zn1) → π*(N25–C18)	15.4
$E^{(2)}d$(Zn1) → π*(N20–N19)	3.3
$E^{(2)}d$(Zn1) → π*(N20–C6)	3.6

[a] Natural charges (q,e) and main second-order perturbation energies ($E^{(2)}$ donor → acceptor, kJ/mol). Computed at the B3LYP/6-31G** level using a relativistic effective core potential for Zn. For the numbering of atoms see Fig. 1.

(+1.60 and +1.61e) and the strong negative character of the pyridine-type nitrogens of the *dmpz* (between −0.55 and −0.59e) and *Hdmpz* (−0.50e) ligands. The slightly less negative character of the *Hdmpz* nitrogen means somewhat weaker electrostatic attractions between this ligand and Zn^{2+} than that with *dmpz*.

The natural charges of the *dmpz* nitrogens support again that the Zn–N interactions cannot be separated into a Zn–N (ionic) single bond and a donor–acceptor interaction. Their minor differences – parallel with the similar Zn–N bond distances – refer to similar bonding properties of the two nitrogens of a *dmpz* with Zn. The large magnitude of the above atomic charges implies a dominant electrostatic attraction between Zn^{2+} and the nitrogens over the donor–acceptor interactions. Summing up the atomic charges within the NCS^- and *dmpz* ligands, we obtained that a Zn^{2+} ion receives ca. 0.1 electron donation from each NCS^-, while less than 0.2 electron from each *dmpz*. This explains that the charge of the zinc ion is only slightly below +2.

The ratio of donation–backdonation within the metal–ligand interactions can be evaluated by analysis of the charge transfer interactions (second-order perturbation energies from the Natural Bond Orbital analysis [41], cf. Table 5). They revealed a moderate (200–250 kJ/mol) charge transfer from *dmpz* to Zn^{2+} while only a marginal (a few kJ/mol) one from Zn^{2+} to the *dmpz* ligands. The charge transfer interactions with the less strongly bound *Hdmpz* ligands are obviously weaker.

3.5. Thermal analysis

The thermal decomposition of the compound was studied in air and argon gas carriers with a heating rate of 10 K/min. The decomposition is continuous in the whole temperature range with three well-defined steps indicated by the DTG peaks at around 350, 550 and 650 K in both air and argon (see Fig. 4). Above 700 K the decomposition in argon continues with a constant, somewhat slower speed and is not complete up to 1000 K. In air one more step is observed in the temperature range of 700–870 K. Above 870 K uncontrollable processes with a slight increase of the mass – presumably a partial oxidation – can be observed. This phenomenon was earlier observed at the decomposition of sulphur containing compounds [4,21,42].

The thermal stability of the complex is rather low and its decomposition starts at 350 K with a clearly distinguishable step. We considered the possibility of desolvation or evolution of ammonia, which take also place at such low temperatures. However, the EGD curve supported the evolution of an organic fragment (see Fig. 5). The mass loss of ca. 3.5% corresponds to the departure of two CH_2 fragments (Calc., 3.16%), most likely from the terminal *Hdmpz* molecules. The loss of a CH_2 radical during an intramolecular rearrangement in 5-methyl pyrazole derivatives has been found previously in coupled TG–MS measurements accompanied with an exothermic process [43]. In some cases 5-methyl pyrazole complexes decomposed giving relatively stable intermediates. The composition and structure of these isolated intermediates was determined by elemental analysis and IR spectroscopy [6,43,44], respectively, supporting the departure of a CH_2 fragment. In the case of the $[Zn_3(Hdmpz)_2(dmpz)_4(NCS)_2]$ complex probably the lower flexibility of the trinuclear core prevents the formation of a stable intermediate.

In the temperature range of 395–555 K (argon) and 395–605 K (air) the mass loss amounts to 33% and 31%, respectively. It corresponds most probably to a leave of the remaining parts of the terminal *Hdmpz* molecules, which is in agreement with the lower dissociation energies computed for the terminal ligands. Parallel with the departure of the *Hdmpz* ligands, a demethylation of the other pyrazole moieties of the complex and/or the loss of NCS groups may be supposed. The following relatively sharp step at about 700 K represents an additional mass loss of about 28 ± 2%, while above this temperature a slow decomposition takes places in both atmospheres. The decomposition product above 870 K may correspond to the zinc-nitride core of the complex (mass found 37%, Calc., 34.82%), which can be pretty stable to slow down the decomposition in both atmospheres, but not stable enough to be isolated for a detailed analysis.

The thermal decomposition of the compound in both atmospheres and in the whole measured temperature range is endothermic. The endothermic peak in the DSC curve with an onset temperature of 350 K, i.e. at the beginning of the decomposition (Fig. 4) is not sharp enough to be

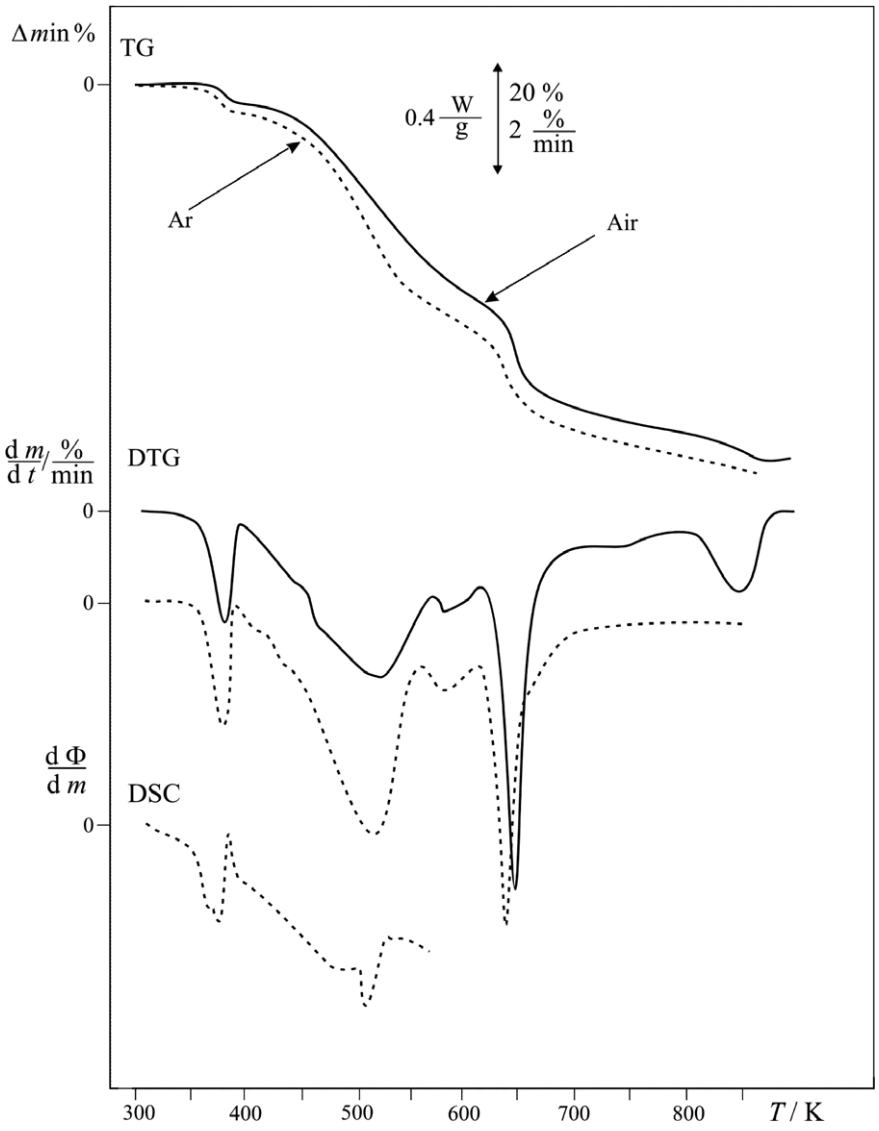

Fig. 4. Thermal decomposition curves of $[Zn_3(Hdmpz)_2(dmpz)_4(NCS)_2]$.

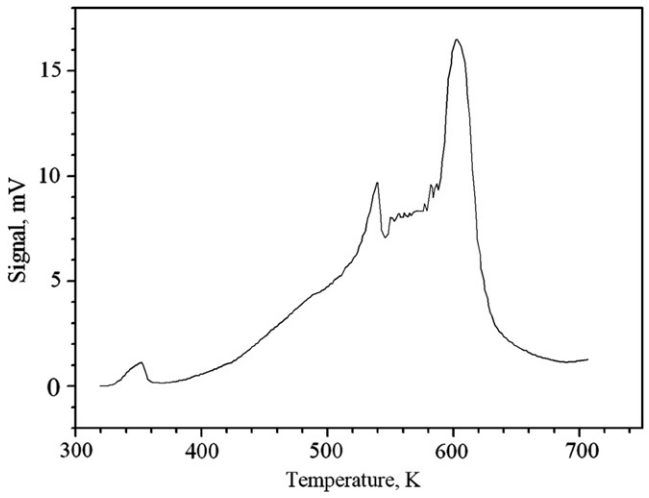

Fig. 5. EGD curve of the complex decomposition.

attributed to the melting of the compound. However, we have visually observed a melting at around this temperature accompanying the decomposition of the complex.

4. Conclusions

The self-controlled pH during the reaction of tetraamminezinc(II) chloride with 3,5-dimethyl-1-thiocarboxamidepyrazole facilitated the synthesis of good quality single crystals of the trinuclear $[Zn_3(Hdmpz)_2(dmpz)_4(NCS)_2]$ complex. Due to the slow initial reaction rate only a few crystal nuclei were formed at the beginning of the reaction, which increased gradually with the increasing pH as NH_3 deliberated from the reacting $[Zn(NH_3)_4]Cl_2$. Even this mild pH supported the cleavage of the thiocarboxamide group from 3,5-dimethyl-1-thiocarboxamidepyrazole. The other consequence of the mild pH is the presence of the

dmpz–Hdmpz equilibrium resulting in a mixed complex. The replacement of chloride by thiocyanate ions around Zn^{2+} during the reaction could be explained upon the different basic character of the ions using the HSAB principle.

The structural properties of the complex were elucidated by X-ray diffraction and quantum chemical computations. Both reflect strong Zn–N ionic and donor–acceptor bonds within the $[Zn_3(dmpz)_4]^{2+}$ core. We determined the vibrational and thermal characteristics of the complex.

Acknowledgements

The authors are grateful to Prof. I. Radosavljević Evans for the X-ray diffraction measurement and advice. The work was financed in part by the Ministry for Science and Environmental Protection of the Republic of Serbia (Grant No.142028) and Provincial Secretariat for Science and Technological Development of Vojvodina. Additional financial support from the Hungarian Scientific Research Foundation (OTKA No. T68332) and computational time from the National Information Infrastructure Development Program of Hungary is gratefully acknowledged. M.Sz.K. thanks the Arany János and A.K. the Bolyai Foundation for support.

Appendix A. Supplementary material

CCDC 622008 contains the supplementary crystallographic data for this paper. These data can be obtained free of charge via http://www.ccdc.cam.ac.uk/conts/retrieving.html, or from the Cambridge Crystallographic Data Centre, 12 Union Road, Cambridge CB2 1EZ, UK; fax: (+44) 1223-336-033; or e-mail: deposit@ccdc.cam.ac.uk.

References

[1] K. Byrappa, T. Ohachi (Eds.), Crystal Growth Technology, Springer, Berlin, 2003.
[2] D.T.J. Hurle (Ed.), Handbook of Crystal Growth: Bulk Crystal Growth, Elsevier, Amsterdam, 1996.
[3] D.A. Skoog, D.M. West, F.J. Holler, Fundamentals of Analytical Chemistry, sixth ed., Saunders College Publishing, 1992 (Croatian edition).
[4] K. Mészáros Szécsényi, V.M. Leovac, A. Kovács, G. Pokol, Ž.K. Jaćimović, J. Therm. Anal. Calorim. 85 (2006) 289.
[5] K. Mészáros Szécsényi, V.M. Leovac, V.I. Češljević, A. Kovács, G. Pokol, Gy. Argay, A. Kálmán, G.A. Bogdanović, Ž.K. Jaćimović, A. Spasojević-de Biré, Inorg. Chim. Acta 353 (2003) 253.
[6] K. Mészáros Szécsényi, V.M. Leovac, Ž.K. Jaćimović, V.I. Češljević, A. Kovács, G. Pokol, J. Therm. Anal. Calorim. 66 (2001) 573.
[7] Kovács D. Nemcsok, G. Pokol, K. Mészáros Szécsényi, V.M. Leovac, Ž.K. Jaćimović, I. Radosavljević Evans, J.A.K. Howard, Z.D. Tomić, G. Giester, New J. Chem. 29 (2005) 833 (and references therein).
[8] G.M. Sheldrick, SADABS, University of Göttingen, Germany, 1998.
[9] SAINT+, Release 6.22. Bruker Analytical Systems, Madison, WI, USA, 1997–2001.
[10] A. Altomare, G. Cascarano, G. Giacovazzo, A. Guagliardi, M.C. Burla, G. Polidori, M. Camalli, J. Appl. Crystallogr. 27 (1994) 435.
[11] P.W. Betteridge, J.R. Carruthers, R.I. Cooper, K. Prout, D.J. Watkin, J. Appl. Crystallogr. 36 (2003) 1487.
[12] M.N. Burnett, C.K. Johnson, ORTEPIII. Report ORNL-6895. Oak Ridge National Laboratory, TN, USA, 1996.
[13] M.J. Frisch, G.W. Trucks, H.B. Schlegel, G.E. Scuseria, M.A. Robb, J.R. Cheeseman, J.A. Montgomery Jr., T. Vreven, K.N. Kudin, J.C. Burant, J.M. Millam, S.S. Iyengar, J. Tomasi, V. Barone, B. Mennucci, M. Cossi, G. Scalmani, N. Rega, G.A. Petersson, H. Nakatsuji, M. Hada, M. Ehara, K. Toyota, R. Fukuda, J. Hasegawa, M. Ishida, T. Nakajima, Y. Honda, O. Kitao, H. Nakai, M. Klene, X. Li, J.E. Knox, H.P. Hratchian, J.B. Cross, C. Adamo, J. Jaramillo, R. Gomperts, R.E. Stratmann, O. Yazyev, A.J. Austin, R. Cammi, C. Pomelli, J.W. Ochterski, P.Y. Ayala, K. Morokuma, G.A. Voth, P. Salvador, J.J. Dannenberg, V.G. Zakrzewski, S. Dapprich, A.D. Daniels, M.C. Strain, O. Farkas, D.K. Malick, A.D. Rabuck, K. Raghavachari, J.B. Foresman, J.V. Ortiz, Q. Cui, A.G. Baboul, S. Clifford, J. Cioslowski, B.B. Stefanov, G. Liu, A. Liashenko, P. Piskorz, I. Komaromi, R.L. Martin, D.J. Fox, T. Keith, M.A. Al-Laham, C.Y. Peng, A. Nanayakkara, M. Challacombe, P.M.W. Gill, B. Johnson, W. Chen, M.W. Wong, C. Gonzalez, J.A. Pople, GAUSSIAN 03, Gaussian Inc., Pittsburgh PA, 2003.
[14] A.D. Becke, J. Chem. Phys. 98 (1993) 5648.
[15] C. Lee, W. Yang, R.G. Parr, Phys. Rev. B 41 (1988) 785.
[16] P.J. Hay, W.R. Wadt, J. Chem. Phys. 82 (1985) 270.
[17] A.W. Ehlers, M. Böhme, S. Dapprich, A. Gobbi, A. Höllwarth, V. Jonas, K.F. Köhler, R. Stegmann, A. Veldkamp, G. Frenking, Chem. Phys. Lett. 208 (1993) 111.
[18] S.F. Boys, F. Bernardi, Mol. Phys. 19 (1970) 553.
[19] T. Barszcz, J. Glowiak, K. Jezierska, K. Kurdziel, Inorg. Chem. Commun. 5 (2002) 1056.
[20] T. Barszcz, J. Glowiak, A. Jezierska, A. Tomkiewicz, Polyhedron 23 (2004) 1309.
[21] K. Mészáros Szécsényi, V.M. Leovac, Ž.K. Jaćimović, G. Pokol, J. Therm. Anal. Calorim. 74 (2003) 943.
[22] R.G. Pearson, J. Am. Chem. Soc. 85 (1963) 3533.
[23] R.G. Pearson, J. Songstad, J. Am. Chem. Soc. 89 (1967) 1827.
[24] T.-L. Ho, Chem. Rev. 75 (1975) 1.
[25] N. Masciocchi, G.A. Ardizzoia, A. Maspero, G. LaMonica, A. Sironi, Inorg. Chem. 38 (1999) 3657.
[26] M.K. Ehlert, S.J. Retting, A. Store, R.C. Thomson, J. Trotter, Can. J. Chem. 68 (1990) 1494.
[27] Z.D. Tomić, Ž.K. Jaćimović, V.M. Leovac, V.I. Češljević, Acta Crystallogr. C 60 (2000) 777.
[28] W.J. Geary, Coord. Chem. Rev. 7 (1971) 81.
[29] T.M. Krygowski, J. Chem. Inf. Comput. Sci. (1993) 70.
[30] Y.-J. Sun, P. Cheng, S.-P. Yan, Z.-H. Jiang, D.-Z. Liao, P.-W. Shen, J. Coord. Chem. (2002) 363.
[31] A. Looney, R. Han, I.B. Gorrell, M. Cornebise, K. Yoon, G. Parkin, A.L. Rheingold, Organometallics 14 (1995) 274.
[32] G. Schaftenaar, Molden 3.8. Centre for Molecular and Biomolecular Informatics, University of Nijmegen, Nijmegen, 2003.
[33] D. Nemcsok, A. Kovács, K. Mészáros Szécsényi, V.M. Leovac, Chem. Phys. 328 (2006) 85.
[34] J.M. Orza, M.V. García, I. Alkorta, J. Elguero, Spectrochim. Acta A 56 (2000) 1469.
[35] K. Nakamoto, Infrared and Raman Spectra of Inorganic and Coordination Compounds. Part B: Applications in Coordination, Organometallic and Bioinorganic Chemistry, Wiley, New York, 1997.
[36] R.A. Bailey, S.L. Kozak, T.W. Michelsen, W.N. Mills, Coord. Chem. Rev. 6 (1971) 407.
[37] A. Anagnostopoulos, J. Inorg. Nucl. Chem. 38 (1976) 435.
[38] A. Szabó, V.I. Češljević, A. Kovács, Chem. Phys. 270 (2001) 67.
[39] D.A. Thornton, Coord. Chem. Rev. 104 (1990) 251.
[40] D.R. Lide (Ed.), CRC Handbook of Chemistry and Physics, 81st ed., CRC Press, Boca Raton, 2000, pp. 9–55.
[41] A.E. Reed, L.A. Curtiss, F. Weinhold, Chem. Rev. 88 (1988) 899.
[42] G. Liptay (Ed.), Atlas of Thermoanalytical Curves, vol. 3, Akademiai Kiadó/Heyden and Sons, Budapest/London, 1974, No. 160.

[43] K. Mészáros Szécsényi, E.Z. Ivegeš, V.M. Leovac, Lj.S. Vojinović, G. Pokol, A. Kovács, J. Madarász, Ž.K. Jaćimović, Thermochim. Acta 316 (1998) 79.

[44] K. Mészáros Szécsényi, E.Z. Ivegeš, V.M. Leovac, A. Kovács, G. Pokol, Ž.K. Jaćimović, J. Therm. Anal. Calorim. 56 (1999) 493.